

## PAPER

# Mutual Coupling Reduction for Dual-Band MIMO Antenna via Artificial Transmission Line

Xiang XIONG<sup>†</sup>, Student Member, Wen LI<sup>†</sup>, Xiaohua TAN<sup>††</sup>, and Yusheng HU<sup>†††a)</sup>, Nonmembers

**SUMMARY** A dual-band decoupling strategy via artificial transmission line (TL) for closely spaced two-element multiple-input multiple-output (MIMO) antenna is proposed, which consists of two composite right-/left-handed TLs for dual-band phase shifting and a cross-shaped TL for susceptance elimination to counteract the real and imaginary part of the mutual coupling coefficient  $S_{21}$  at dual frequency bands, respectively. The decoupling principle and detailed design process of the dual-band decoupling scheme are presented. To validate the dual-band decoupling technique, a closely spaced dual-band MIMO antenna for 5G (sub-6G frequency band) utilization is designed, fabricated, and tested. The experimental results agree well with the simulation ones. A dual-band of 3.40 GHz–3.59 GHz and 4.79 GHz–4.99 GHz ( $S_{11}$  &  $S_{22} < -10$  dB,  $S_{12}$  &  $S_{21} < -20$  dB) has been achieved, and the mutual coupling coefficient  $S_{21}$  is significantly reduced 21 dB and 16.1 dB at 3.5 GHz and 4.9 GHz, respectively. In addition, the proposed dual-band decoupling scheme is antenna independent, and it is very suitable for other tightly coupled dual-band MIMO antennas.

**key words:** composite right-/left-handed transmission line, cross-shaped TL, dual-band decoupling, multiple-input multiple-output (MIMO), mutual coupling

## 1. Introduction

Multiple-input multiple-output (MIMO) antenna technique exhibits fairly good properties with high data throughput and low time transmission delay, which has been universally adopted in 5G and radar systems [1]. However, the miniaturization trend in modern wireless systems making the antenna design still needs to consider the limited space available for mounting multiple antennas. Severe electromagnetic (EM) coupling would occur if the inter-element distance is less than half of the operating wavelength in free space. The strong EM coupling not only has effects on the radiation efficiency of the MIMO antenna but also declines the working capability in engineering applications for the MIMO antenna.

To solve the technical contradiction mentioned above, several methodologies have been presented for EM coupling reduction. Neutralization-line technique [2], [3] is a common decoupling approach, which aims to generate an oppo-

site coupling current to cancel the mutual coupling for the MIMO antenna. Although the neutralization-line technique can reduce EM coupling, to the best of the author's knowledge this way is essentially based on experimental attempts and it is difficult to find a specific design criteria to use now.

Defected ground structure (DGS) [4], [5] can be also used to increase the isolation between MIMO antenna elements. However, the DGS is typically etched from the ground plane, it will destroy the integrity of the ground plane and not benefit the back-radiation performance of the decoupled MIMO antennas.

Metamaterial (MTM) is an engineered structure and possesses many interesting EM characteristics, such as negative permittivity or negative permeability [6], [7]. Electromagnetic bandgap structures (EBG) [8], [9], MTM-photonic bandgap [10], capacitively-loaded loop [11], [12], and metasurface [13], [14] are different formats of MTM. In virtue of the extraordinary characteristics of MTM, the propagation of the surface wave can be prevented to alleviate the EM coupling among the adjacent antenna elements [8]–[15]. However, the design process of MTM is relatively complex and it always occupies a large volume which will dramatically increase the package size of the communication system.

The decoupling and matching network (DMN) [16]–[19] can furnish an effective and systematic way to mitigate the EM coupling and improve the isolation in an array of MIMO systems. The working mechanism of the DMN is to remove the real part of the coupling coefficient  $S_{21}$  by utilizing a section of transmission line (TL), and then, a well designed anti-susceptance is designed to vanish the imaginary part of the coupling coefficient and enhance the isolation for the coupled MIMO antenna [19]. However, the traditional DMNs [18]–[20] are limited in single-band decoupling due to the linear phase response of the TL, which is not consistent with the trend of dual-band or multi-band wireless systems. In order to tackle this problem, some dual-band decoupling methods have been reported in [21]–[25], such as the dual-band rat-race coupler in [22], the multipath decoupling circuit in [24], and the hybrid resonant structure in [25], et al. Though the aforementioned dual-band decoupling scheme achieves a good mutual coupling reduction, some problems still exist, for instance, the narrow operating band or the center-to-center space between antenna elements is actually large.

In this work, a dual-band decoupling strategy is presented and investigated for the closely spaced two-element dual-band MIMO antenna, which consists of two composite

Manuscript received January 7, 2024.

Manuscript revised April 15, 2024.

Manuscript publicized June 11, 2024.

<sup>†</sup>College of Information and Communication Engineering, Harbin Engineering University, Harbin 150001 P.R. China.

<sup>††</sup>Beijing Key Laboratory of Work Safety Intelligent Monitoring, School of Electronic Engineering, Beijing University of Posts and Telecommunications, Beijing 100876 P.R. China.

<sup>†††</sup>College of Marine Equipment and Mechanical Engineering, Jimei University, Xiamen 361021 P.R. China.

a) E-mail: hysmk@sina.com (Corresponding author)

DOI: 10.1587/transle.2024ECP5001

right/left-handed (CRLH) TLs and a cross-shaped TL. The CRLH-TL with nonlinear phase response is utilized for dual-band phase shifting to eliminate the real part of the coupling coefficient  $S_{21}$ . After that, a cross-shaped TL is employed to counteract the imaginary part of  $S_{21}$  at dual frequency band, then to decouple the dual-band MIMO antenna. The decoupling principle and design process of this methodology are given in Sect. 2. To validate the proposed decoupling scheme, a closely spaced dual-band MIMO antenna for 5G (sub-6G) utilization is designed, fabricated, and analyzed in Sect. 3. In final, the conclusions are drawn in Sect. 4.

## 2. Dual-Band Decoupling Scheme and Theory Analysis

### 2.1 The Proposed Dual-Band Decoupling Scheme

As is known, for a closely spaced two-element dual-band MIMO antenna given in Fig. 1, impedance matching is much easier than decoupling. Assuming the the closely spaced two-element MIMO antenna matches their port input impedance  $Z_0$  very well at the reference plane T1 but suffers severe EM coupling. Then, the coupled S-parameter matrix of the two-port network for the two-element MIMO antenna at the reference plane T1 can be approximately expressed as

$$[S^{T1}] = \begin{bmatrix} 0 & |S_{12}^{T1}(\omega)| e^{j\phi^{T1}(\omega)} \\ |S_{21}^{T1}(\omega)| e^{j\phi^{T1}(\omega)} & 0 \end{bmatrix}, \quad (1)$$

where  $|S_{12}^{T1}(\omega)|$  and  $|S_{21}^{T1}(\omega)|$  denote the magnitude, while  $\phi^{T1}(\omega)$  represents the phase of insertion loss of the two port network at T1 plane. Typically, the insertion loss ( $S_{12} = S_{21}$ ) stands for the levels of the EM mutual coupling between two MIMO antenna elements, with a higher value of  $S_{21}$  indicating a stronger degree of coupling.

As depicted in Fig. 1, the dual-band decoupling scheme is composed of two CRLH-TLs and a cross-shaped TL to eliminate the real and imaginary part of the mutual coupling coefficient  $S_{21}$ , respectively, at the lower resonance frequency  $\omega_L$  and upper resonance frequency  $\omega_H$  ( $\omega_L < \omega_H$ ). To eliminate the real part of the  $S_{21}$ , the characteristic impedance of the CRLH-TL added at the T1 plane should keep the same with the port input impedance  $Z_0$  and according to the TL theory [26], the electric length of the CRLH-TL at the two resonance frequencies should follow as:

$$\theta_L = \frac{1}{2} \left[ \phi^{T1}(\omega_L) \pm \frac{\pi}{2} + k\pi \right], k \in Z, \quad (2a)$$

$$\theta_H = \frac{1}{2} \left[ \phi^{T1}(\omega_H) \pm \frac{\pi}{2} + k\pi \right], k \in Z, \quad (2b)$$

where  $Z$  denotes an integer set,  $\theta_L$  and  $\theta_H$  represent the electric length of the CRLH-TL at two resonance frequencies  $\omega_L$  and  $\omega_H$  respectively. After that, the S-parameter matrix of the two-port network at reference plane T2 can be converted into the corresponding admittance matrix  $[Y^{T2}]$  [26], that is

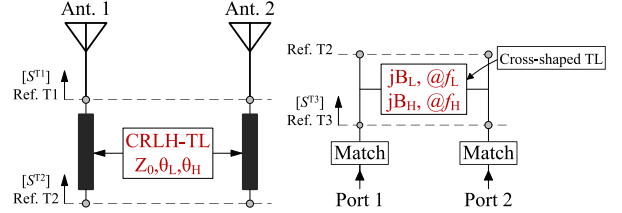


**Fig. 1** Schematic of the proposed dual-band decoupling scheme.

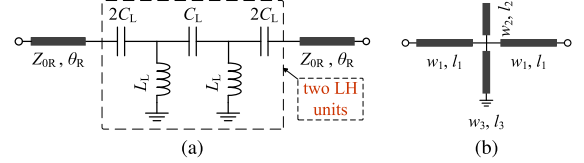


**Fig. 2** (a) The equivalent circuit of the CRLH-TL for dual-band phase shifting. (b) Cross-shaped TL for dual-band susceptance counteracting.

$$[Y_L^{T2}] = \frac{1}{Z_0} \begin{bmatrix} \frac{1 \mp |S_{21}^{T1}(\omega_L)|^2}{1 \pm |S_{21}^{T1}(\omega_L)|^2} & \frac{\mp j2|S_{21}^{T1}(\omega_L)|}{1 + |S_{21}^{T1}(\omega_L)|^2} \\ \frac{\mp j2|S_{21}^{T1}(\omega_L)|}{1 + |S_{21}^{T1}(\omega_L)|^2} & \frac{1 \mp |S_{21}^{T1}(\omega_L)|^2}{1 \pm |S_{21}^{T1}(\omega_L)|^2} \end{bmatrix}, \quad (3a)$$

$$[Y_H^{T2}] = \frac{1}{Z_0} \begin{bmatrix} \frac{1 \mp |S_{21}^{T1}(\omega_H)|^2}{1 \pm |S_{21}^{T1}(\omega_H)|^2} & \frac{\mp j2|S_{21}^{T1}(\omega_H)|}{1 + |S_{21}^{T1}(\omega_H)|^2} \\ \frac{\mp j2|S_{21}^{T1}(\omega_H)|}{1 + |S_{21}^{T1}(\omega_H)|^2} & \frac{1 \mp |S_{21}^{T1}(\omega_H)|^2}{1 \pm |S_{21}^{T1}(\omega_H)|^2} \end{bmatrix}. \quad (3b)$$

Once the real part of the  $S_{21}$  is vanished, as illustrated in Fig. 1, the cross-shaped TL is in shunted at the reference plane T2. It will provide two reactive elements of susceptance  $jB_L$  and  $jB_H$  to eliminate the imaginary part of  $S_{21}$  at two resonance frequencies  $\omega_L$  and  $\omega_H$ , respectively. The susceptance  $jB_L$  and  $jB_H$  should be equal to the inverse of the transfer admittance of  $[Y^{T2}]$  at two resonance frequencies  $\omega_L$  and  $\omega_H$ , namely

$$B_L = \frac{1}{Z_0} \frac{\pm 2|S_{21}^{T1}(\omega_L)|}{1 + |S_{21}^{T1}(\omega_L)|^2}, B_H = \frac{1}{Z_0} \frac{\pm 2|S_{21}^{T1}(\omega_H)|}{1 + |S_{21}^{T1}(\omega_H)|^2}. \quad (4)$$

### 2.2 The CRLH-TL for Dual-Band Phase Shifting

The CRLH-TL is employed for dual-band phase shifting to eliminate the real part of  $S_{21}$  and whose equivalent circuit model is shown in Fig. 2 (a) [22], [27], [28]. With respect to the LH part of the CRLH-TL, which is formed by two series capacitors ( $2C_L$ ) along with a shunt inductor ( $L_L$ ) inserted in-between. Because the phase response of LH-TL is positive (phase advance), it is utilized to combine the RH-TL (phase lag) to exhibit nonlinear phase response at two desired frequency bands. Then, the CRLH-TL is employed for dual-band phase shifting to eliminate the real part of  $S_{21}$  at the lower and upper bands. According to [27], the unit phase responses for the RH-TL and LH-TL are

$$\phi_{\text{unit}}^L = -\arctan \left[ \omega \frac{C_L Z_{0L} + \frac{L_L}{Z_{0L}} - \frac{1}{4\omega^2 C_L Z_{0L}}}{1 - 2\omega^2 C_L L_L} \right], \quad (5a)$$



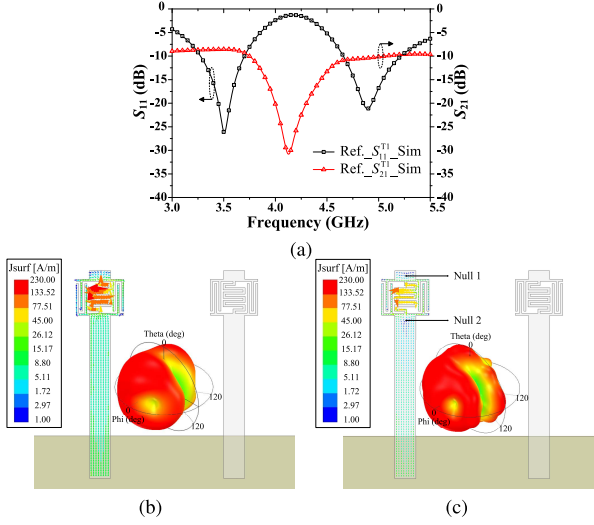


**Fig. 4** (a) Simulated S-parameters of the reference MIMO antenna. The current distribution on the monopole antenna element and its related 3D radiation pattern at (b) 3.5 GHz. (c) 4.9 GHz.

4.66 GHz to 5.22 GHz). In addition, Fig. 4 (b) and (c) also illustrate the current distribution on the monopole and its related 3D radiation pattern. It is found most of the current at 3.5 GHz propagates along stripline  $l_{a1}$ , meander line inductor, and then reaches the end of the monopole, which will precipitate the radiation at the lower frequency band. While at 4.9 GHz, two null current points appear at Null 1 and Null 2, which confirms the resonance in the LC parallel circuit, consequently, stripline  $l_{a2}$  will dominate the radiation at the upper frequency band.

Since the center-to-center distance (CCD) of two antenna elements is only 9.5 mm, which is about  $0.11 \lambda_L$  ( $\lambda_L$  represents the free-space wavelength at 3.5 GHz), it will make the antenna elements suffer severe EM coupling. As depicted in Fig. 4, the simulated mutual coupling coefficient  $S_{21}$  reaches up to  $-8.54$  dB and  $-10.39$  dB at 3.5 GHz and 4.9 GHz, respectively. Evidently, the isolation for the reference MIMO antenna is not acceptable, therefore, much attention should be paid to the EM coupling reduction among the adjacent antenna elements, and a dual-band decoupling strategy is desperately required.

### 3.2 Phase Shifting and Susceptance Elimination for $S_{21}$

For a given closely spaced two-element monopole MIMO antenna, the S-parameters matrix  $[S^{T1}]$  at the reference plane T1 is defined. The CRLH-TL with characteristic impedance  $Z_0$  is added at reference plane T1 to realize phase shifting and eliminate the real part of  $S_{21}$  at dual frequency bands. As shown in Fig. 5 (a), the phase of  $S_{21}$  for the reference MIMO antenna without adding CRLH-TL at T1 plane is  $-102.87^\circ$  and  $-109.31^\circ$  at 3.5 GHz and 4.9 GHz, respectively. According to Eq. (2), the electric length of the CRLH-TL ( $\theta_L$  and  $\theta_H$ ) for phase shifting can be obtained, and it is  $83.56^\circ$  and  $170.35^\circ$  when  $k$  is chosen to be 1 and 2 at Eq. (2) (a) and Eq. (2) (b), respectively. Following the design rule pro-

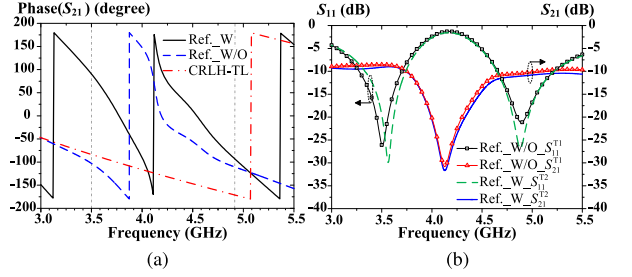


**Fig. 5** (a) Phase of  $S_{21}$  for the reference MIMO antenna with and without adding CRLH-TL at T1 plane and the phase of  $S_{21}$  for CRLH-TL itself. (b) S-parameters of the reference MIMO antenna with and without CRLH-TL integration at T1 plane.

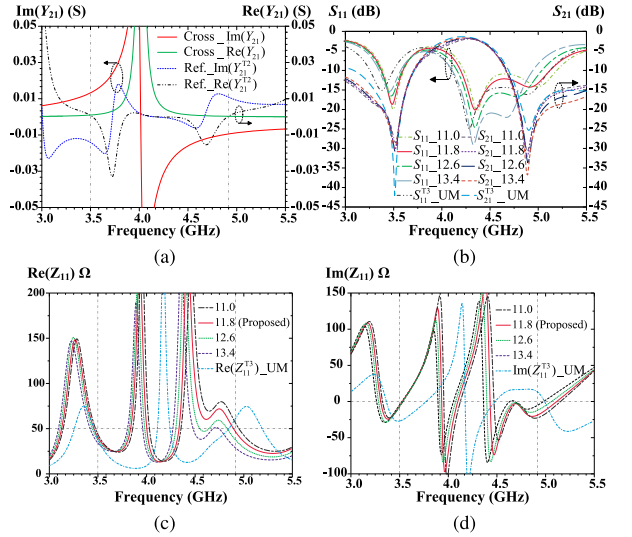


**Fig. 6** (a) Simulated  $Y_{21}$  of the cross-shaped TL and those of the reference MIMO antenna with CRLH-TL integration at T2 plane. Simulated (b) S-parameters, (c) real and (d) imaginary part of  $Z_{11}$  with different  $l_{m2}$  during the impedance matching process.

posed in Sect. 2.2, the circuit parameters of the CRLH-TL ( $L_L$ ,  $C_H$  and  $\theta_R$ ) depicted in Fig. 2 (a) can be calculated from Eqs. (6)–(9), which are 3.35 nH, 1.34 pF, and  $80.68^\circ$ .

Figure 5 (a) reveals the phase response of the CRLH-TL simulated by the Keysight ADS. The simulation values at two resonance frequencies  $\omega_L$  (3.5 GHz) and  $\omega_H$  (4.9 GHz) are  $-83.5^\circ$  and  $-170.3^\circ$ , which closely match the calculated values by Eq. (2). Though the circuit values in ADS have been slightly tuned to 3.4 nH, 1.4 pF, and  $80.18^\circ$  for realizing consideration. The phase response of  $S_{21}$  of the reference MIMO antenna with adding two CRLH-TLs at T2 plane is also given in Fig. 5 (a), and it is  $90.46^\circ$  and  $-89.89^\circ$ , respectively when it operates at 3.5 GHz and 4.9 GHz, which means the real part of  $S_{21}$  is vanished after the dual-band phase shifting. Figure 5 (b) shows the effects on the S-parameters before and after phase shifting for  $S_{21}$ , it is found that there is no important influence on the impedance bandwidth and mutual coupling coefficient  $S_{21}$ . Though a slightly offsetting at the low band is found, the  $-10$  dB impedance BW still covers from 3.33 GHz to 3.74 GHz.

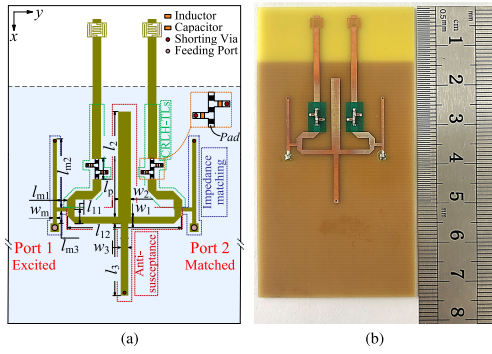


**Fig. 7** (a) Layout and (b) prototype of the decoupled monopole MIMO antenna with  $w_1 = 1.2$ ,  $w_2 = 2.2$ ,  $w_3 = 1.3$ ,  $w_m = 0.7$ ,  $l_{11} = 2.45$ ,  $l_{12} = 19.6$ ,  $l_2 = 18.1$ ,  $l_3 = 12.4$ ,  $l_{m1} = 1.7$ ,  $l_{m2} = 11.8$ ,  $l_{m3} = 2.05$  (unit: mm).

Once the real part of  $S_{21}$  is dispelled, as depicted in Fig. 6 (a), the transfer admittance  $Y_{21}$  of the reference MIMO antenna at T2 plane are  $0 - j0.0141\text{S}$  and  $0 + j0.0113\text{S}$  at 3.5 GHz and 4.9 GHz respectively. The cross-shaped TL is considered to provide the inverse of the transfer admittance  $Y_{21}$  to wipe off the imaginary part of  $S_{21}$  and decouple the reference MIMO antenna at dual-frequency band. As mentioned in Sect. 2.3, it is difficult to obtain an analytic solution for Eq. (4). But the function of optimization in Keysight ADS can provide an iterative solution, and the parameters of the cross-shaped TL iterated by ADS are  $0.8(w_1)$ ,  $2.2(w_2)$ ,  $1.3(w_3)$ ,  $9.4(l_1)$ ,  $18.1(l_2)$ ,  $11.3(l_3)$ , (unit: mm). However, the  $Y_{21}$  obtained by ADS at 3.5 GHz and 4.9 GHz are  $+j0.007\text{S}$  ( $jB_L$ ) and  $-j0.011\text{S}$  ( $jB_H$ ), which is not good enough to provide the anti-susceptance at the lower frequency band. To make the imaginary part of  $Y_{21}$  as closely as possible to  $+j0.0141\text{S}$  and  $-j0.0113\text{S}$  at 3.5 GHz and 4.9 GHz. Further optimization of the cross-shaped TL is conducted in ANSYS HFSS, as shown in Fig. 6 (a), the final optimized  $Y_{21}$  values at those frequencies are  $+j0.0133\text{S}$  and  $-j0.0096\text{S}$ . The layout and parameters of the cross-shaped TL utilized in HFSS are depicted in Fig. 7 (a).

After that, the dual-band reference MIMO antenna is decoupled and the related S-parameters at T3 plane is illustrated in Fig. 6 (b) (gray dash dot dot line line). It can be seen the resonance point at the lower band has been slightly shifted. In addition, the resonance dip observed at  $S_{11}$  below  $-10\text{dB}$  around the 4.25 GHz band primarily originates the  $Y_{11}$  of cross-shaped TL, but the peak gain of the decoupled MIMO antenna in this band is very low and the filter among the transceiver system and power amplifier will guarantee the undesired signal flow to communication system. To realize the input impedance matches at dual-frequency band, the grounded stub with a length of  $l_{m2}$  is inserted in-between a TL to adjust the input impedance of the decoupled MIMO antenna at T3 plane. Figure 6 (c) and (d) illustrate the effects of  $l_{m2}$  (from 11 to 13.4 mm) on the real and imaginary of the input impedance. When  $l_{m2}$  was tuned to 11.8 mm, an optimal input impedance at dual-band is obtained.

The layout and ultimate dimensions of the decoupled monopole MIMO antenna are depicted in Fig. 7 (a). With

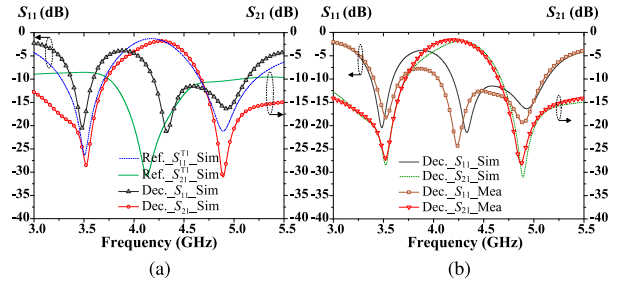


**Fig. 8** (a) Simulated S-parameters for the reference and decoupled monopole MIMO antenna. (b) Simulated and measured S-parameters of the decoupled monopole MIMO antenna.

respect to the layout of the decoupled monopole MIMO antenna, it is worth mentioning that a post-tuning process of the circuit parameters for the CRLH-TL is needed, due to the inductor of vias ( $\phi = 0.5\text{mm}$ ), the electrical length of pads ( $0.6\text{mm} \times 0.4\text{mm}$ ) and the capacitive coupling effect between adjacent pads are not taken into account in circuit simulation. The final circuit parameters of the CRLH-TL are  $L_L = 3.3\text{nH}$ ,  $C_H = 1.1\text{pF}$ , and  $\theta_R = 70.68^\circ$ , respectively. Figure 8 (a) shows the simulated results comparison of the two-port S-parameters between the reference and decoupled monopole MIMO antenna. Compared with the reference antenna, the mutual coupling coefficient  $S_{21}$  is improved by 20 dB at two center resonance frequencies (3.5 GHz and 4.9 GHz). Furthermore, the isolation  $S_{21}$  of two ports drops to below  $-20\text{dB}$  at both two frequency bands (3.39 GHz–3.59 GHz, 4.81 GHz–5.01 GHz). Meanwhile, the reflection coefficient  $S_{11}$  is better than  $-10\text{dB}$  and the CCD of two antenna elements is only  $0.11\lambda_L$ , showing good performance of the proposed dual-band decoupling scheme.

### 3.3 Performances of the Decoupled MIMO Antenna Array

#### 3.3.1 S-Parameters

To further validate the decoupling performance of the proposed dual-band decoupling strategy used in the closely spaced two-element dual-band MIMO antenna, a prototype of the decoupled monopole array is fabricated and presented in Fig. 7 (b). Herein, the Murata surface mount technology (SMT) chip components with a package size of 0402 ( $1\text{mm} \times 0.5\text{mm}$ ) are adopted to make up the LH part of the CRLH-TL, and the Agilent N5244A vector network analyzer is employed to test the two-port S-parameter of the decoupled monopole array. As depicted in Fig. 8 (b), the measured results are well consistent with the simulation ones. The discrepancy, specifically the slight frequency shifting in the upper band, can originate from the fabrication tolerance and the variation of the dielectric constant of the FR4 substrate.

#### 3.3.2 Envelope Correlation Coefficient and Diversity Gain

The envelope correlation coefficient (ECC) is a crucial parameter to evaluate channel isolation for a MIMO antenna,

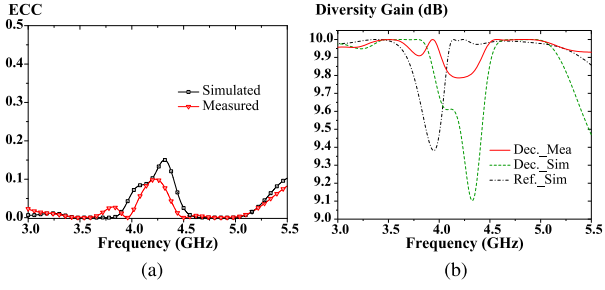


**Fig. 9** (a) Simulated and measured envelope correlation coefficient of the decoupled monopole MIMO antenna. (b) Diversity gain for the decoupled and reference monopole MIMO antenna.

which can be derived from either the radiation patterns or S-parameters. In this work, for simplicity, ECC calculated by the S-parameters is chosen [5]. According to the definition of ECC for two-port S-parameters, it is

$$\text{ECC}(\rho_e) = \frac{|S_{11}^* S_{12} + S_{21}^* S_{22}|^2}{(1 - |S_{11}|^2 - |S_{21}|^2)(1 - |S_{22}|^2 - |S_{12}|^2)}. \quad (10)$$

As illustrated in Fig. 9 (a), the simulated and measured ECCs of the decoupled monopole MIMO antenna are all below 0.05 at both interested frequency bands, which are much lower than the criterion for practice to use ( $\text{ECC} < 0.5$ ) [5]. It means that pretty good isolation is achieved by employing the proposed dual-band decoupling strategy.

For a well-decoupled MIMO system, the diversity gain (DG) can be utilized to estimate the diversity performance for weakly correlated MIMO antenna elements. Supposing the well-matched two-element MIMO antenna is lossless and in a uniform/isotropic random field case (the receiving antenna is under the same condition), DG can be inferred by the ECC calculated above as [25], [30]:

$$\text{DG} = 10\sqrt{1 - \text{ECC}(\rho_e)}. \quad (11)$$

As depicted in Fig. 9 (b), the performance of the DG for the well-decoupled MIMO antenna array approaches 10 dB at both interested frequency bands, which is evidently better than the reference one. At the same time, the DG of the decoupled MIMO antenna is inferior to that of the reference antenna ranging from 4.1 GHz to 4.5 GHz, this is because the isolation of the decoupled MIMO antenna is less effective to the reference one, despite the reflection coefficient of the decoupled MIMO antenna being lower than  $-10$  dB.

### 3.3.3 TRAC and Capacity Loss

It is well known that the traditional S-parameter matrix can not precisely describe the bandwidth for a MIMO antenna system, however, the total active reflection coefficient (TARC) takes the influence of the mutual coupling and incident wave phase into account, which is a better choice to characterize the performance of the whole MIMO antenna

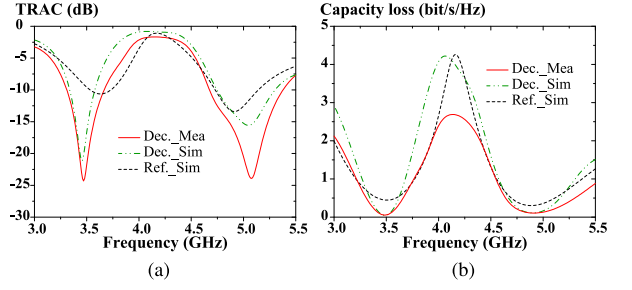


**Fig. 10** Simulated and measured (a) total active reflection coefficient (TRAC), and (b) capacitance loss (CL) for referenced and decoupled monopole MIMO antenna.

array [9], [25], [30]. The TARC can be calculated by

$$\Gamma_a^t = \sqrt{\left( |(S_{11} + S_{12}e^{j\theta})|^2 + |(S_{21} + S_{22}e^{j\theta})|^2 \right) / \sqrt{2}}, \quad (12)$$

where  $\theta$  is the excitation phase angle.

Under the high signal-to-noise ratio circumstances, the channel capacity loss (CL) induced by the correlation matrix can be obtained as

$$\text{CL} = -\log_2 \det(\psi^R), \quad (13)$$

where  $\psi^R$  is the correlation matrix for a two-element MIMO antenna system, and the elements belonging to the correlation matrix can be inferred from

$$\psi_{ii} = 1 - (|S_{ii}|^2 + |S_{ij}|^2), i \neq j = 1, 2, \quad (14a)$$

$$\psi_{ij} = -\left( S_{ii}^* S_{ij} + S_{ji}^* S_{jj} \right), i \neq j = 1, 2. \quad (14b)$$

As illustrated in Fig. 10, the tendency of the TRAC for the decoupled MIMO antenna and the reference antenna is similar to its S-parameters respectively. In the meantime, the CL of the decoupled MIMO antenna array is better than the referenced one at both two interested frequency bands.

### 3.3.4 Radiation Patterns and Peak Gain

Figure 11 depicts the simulated and measured normalized far-field radiation patterns of the decoupled monopole MIMO antenna at 3.5 GHz and 4.9 GHz in the  $xoz$  plane and  $yozy$  plane, respectively. During the testing process, we keep one port (port1) of the MIMO antenna array activated while the other one (port 2) is terminated by a 50-ohm matching load. The radiation patterns of the decoupled monopole MIMO antenna are quasi-omnidirectional and the measured peak gain of the decoupled monopole MIMO antenna are basically same as the simulated ones at both frequency bands, as shown in Fig. 12.

### 3.3.5 Decoupling Performance Comparison

In order to show the decoupling performance of the proposed dual-band decoupling strategy, a comparison list with

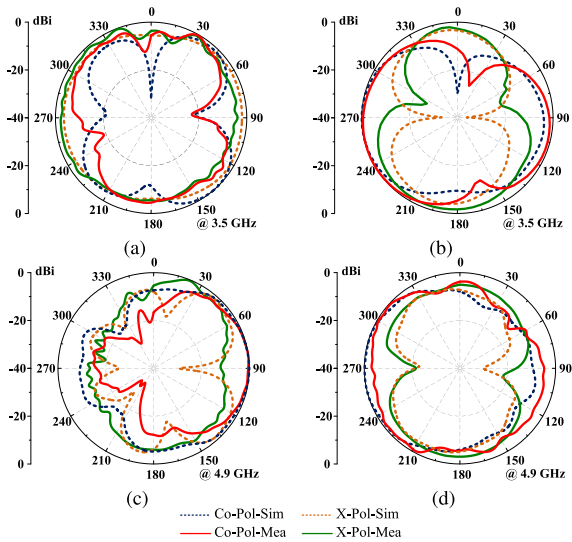


**Fig. 11** Radiation patterns of the decoupled monopole MIMO antenna at (a) 3.5 GHz in  $xoz$  plane. (b) 3.5 GHz in  $yo z$  plane. (c) 4.9 GHz in  $xoz$  plane. (d) 4.9 GHz in  $yo z$  plane.

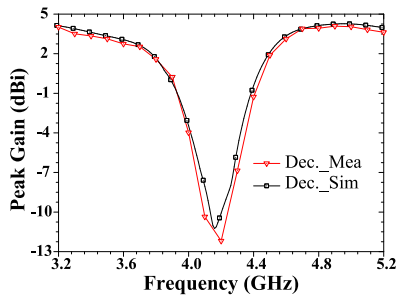


**Fig. 12** Simulated and measured peak gain of the decoupled monopole MIMO antenna.

**Table 1** Performance comparisons with the previous publications.

Ref.	Method	Frequency (GHz)	Achieved BW (%)	CCD ( $\lambda_L, \lambda_H$ )
[9]	EBG	3.48, 4.88	5.1, 8.1	0.46, 0.65
[21]	TLDN	2.45, 5.25	4.0, 4.2	0.09, 0.20
[23]	Metal strips	2.4, 5.1	5.4, 3.7	N. A.
[24]	Decoupling circuit	2.45, 5.77	9.1, 2.6	0.18, 0.43
[25]	Resonant structure	4.5, 5.5	2.2, 1.8	0.45, 0.55
This	Artificial TL	3.5, 4.9	5.4, 4.1	0.11, 0.16

different dual-band decoupling methods is listed in Table 1. Compared with the EBG in [9], TLDN in [21], Metal strips in [23], decoupling circuits in [24], and resonant structure in [25], the proposed dual-band MIMO antenna shows better decoupling performance in the achieved BW ( $S_{11}$  &  $S_{22} < -10$  dB,  $S_{12}$  &  $S_{21} < -20$  dB) and CCD between the antenna elements at both interested bands.

#### 4. Conclusion and Discussion

In this work, a dual-band decoupling strategy for two-element closely spaced MIMO antenna is proposed, which

consists of two CRLH-TLs and a cross-shaped TL. The CRLH-TL with nonlinear phase response is employed to eliminate the real part of  $S_{21}$ , while the cross-shaped TL will provide anti-susceptance to counteract the imaginary part of  $S_{21}$  to decouple the MIMO antenna at both frequency bands. A 5G (sub-6G) dual-band monopole MIMO antenna is designed, decoupled, and fabricated, the measured results agree well with the simulation ones. The decoupled antenna prototype achieves a dual-band of 3.40 GHz–3.59 GHz and 4.79 GHz–4.99 GHz, moreover, the center-to-center space between antenna elements is only  $0.11\lambda_L$  at 3.5 GHz, showing good decoupling performance for closely spaced dual-band MIMO antenna. Besides, the proposed dual-band decoupling method is based on the two-port S-parameters matrix, which is antenna independent and can be expanded to decouple other dual-band two-element MIMO antenna.

#### Acknowledgments

The authors would like to express their gratitude for the generous support by the National Nature Science Foundation of China under Grant 61871200.

#### References

- [1] S. Mahboob and R.G. Vaughan, "Fiber-fed distributed antenna system in an FPGA software defined radio for 5G demonstration," *IEEE Trans. Circuits Syst. II, Exp. Briefs*, vol.67, no.2, pp.280–284, 2020.
- [2] S.-W. Su, C.-T. Lee, and F.-S. Chang, "Printed MIMO-antenna system using neutralization-line technique for wireless USB-dongle applications," *IEEE Trans. Antennas Propag.*, vol.60, no.2, pp.456–463, 2012.
- [3] A. Diallo, C. Luxey, P. Le Thuc, R. Staraj, and G. Kossiavas, "Study and reduction of the mutual coupling between two mobile phone PIFAs operating in the DCS1800 and UMTS bands," *IEEE Trans. Antennas Propag.*, vol.54, no.11, pp.3063–3074, 2006.
- [4] M.S. Sharawi, A.B. Numan, M.U. Khan, and D.N. Alofi, "A dual-element dual-band MIMO antenna system with enhanced isolation for mobile terminals," *IEEE Antennas Wireless Propag. Lett.*, vol.11, pp.1006–1009, 2012.
- [5] W. Wang, Y. Wu, W. Wang, and Y. Yang, "Isolation enhancement in dual-band monopole antenna for 5G applications," *IEEE Trans. Circuits Syst. II, Exp. Briefs*, vol.68, no.6, pp.1867–1871, 2021.
- [6] D.R. Smith, S. Schultz, P. Markoš, and C.M. Soukoulis, "Determination of effective permittivity and permeability of metamaterials from reflection and transmission coefficients," *Phys. Rev. B*, vol.65, no.19, pp.195104, 2002.
- [7] R. Mark, H.V. Singh, K. Mandal, and S. Das, "Mutual coupling reduction using near-zero  $\epsilon$  and  $\mu$  metamaterial-based superstrate for an MIMO application," *IET Microw. Antennas Propag.*, vol.14, no.6, pp.479–484, 2020.
- [8] S. Ghosh, T.-N. Tran, and T. Le-Ngoc, "Dual-Layer EBG-Based Miniaturized Multi-Element Antenna for MIMO Systems," *IEEE Trans. Antennas Propag.*, vol.62, no.8, pp.3985–3997, 2014.
- [9] X. Tan, W. Wang, Y. Wu, Y. Liu, and A.A. Kishk, "Enhancing isolation in dual-band meander-line multiple antenna by employing split EBG structure," *IEEE Trans. Antennas Propag.*, vol.67, no.4, pp.2769–2774, 2019.
- [10] M. Alibakhshikenari, B.S. Virdee, P. Shukla, C.H. See, R.A. Abd-Alhameed, F. Falcone, K. Quazzane, and E. Limiti, "Isolation enhancement of densely packed array antennas with periodic MTM-photonic bandgap for SAR and MIMO systems," *IET Microw. Antennas Propag.*, vol.14, no.3, pp.183–188, 2020.

- [11] A. Jafarholi, A. Jafarholi, and J.H. Choi, "Mutual coupling reduction in an array of patch antennas using CLL metamaterial superstrate for MIMO applications," *IEEE Trans. Antennas Propag.*, vol.67, no.1, pp.179–189, 2019.
- [12] D.A. Ketzaki and T.V. Yioultis, "Metamaterial-based design of planar compact MIMO monopoles," *IEEE Trans. Antennas Propag.*, vol.61, no.5, pp.2758–2766, 2013.
- [13] H. Luan, C. Chen, W. Chen, L. Zhou, H. Zhang, and Z. Zhang, "Mutual coupling reduction of closely E/H-plane coupled antennas through metasurfaces," *IEEE Antennas Wireless Propag. Lett.*, vol.18, no.10, pp.1996–2000, 2019.
- [14] B. Yin and S. Zhao, "Isolation improvement of compact microbase station antenna based on metasurface spatial filtering," *IEEE Trans. Electromagn. Compat.*, vol.63, no.1, pp.57–65, 2021.
- [15] P. Garg and P. Jain, "Isolation improvement of MIMO antenna using a novel flower shaped metamaterial absorber at 5.5 GHz WiMAX band," *IEEE Trans. Circuits Syst. II, Exp. Briefs*, vol.67, no.4, pp.675–679, 2020.
- [16] J.C. Coetzee and Y. Yu, "Design of Decoupling networks for circulant symmetric antenna arrays," *IEEE Antennas Wireless Propag. Lett.*, vol.8, pp.291–294, 2008.
- [17] S.-C. Chen, Y.-S. Wang, and S.-J. Chung, "A decoupling technique for increasing the port isolation between two strongly coupled antennas," *IEEE Trans. Antennas Propag.*, vol.56, no.12, pp.3650–3658, 2008.
- [18] M.A. Moharram and A.A. Kishk, "General decoupling network design between two coupled antennas for MIMO applications," *PIER Letters*, vol.37, pp.133–142, 2013.
- [19] C.-H. Wu, C.-L. Chiu, and T.-G. Ma, "Very compact fully lumped decoupling network for a coupled two-element array," *IEEE Antennas Wireless Propag. Lett.*, vol.15, pp.158–161, 2016.
- [20] H.V. Singh, S. Tripathi, and A. Mohan, "Closely-coupled MIMO antenna with high wideband isolation using decoupling circuit," *AEU-Int. J. Electron. Commun.*, vol.138, pp.153833, 2021.
- [21] N.K. Kiem and D.N. Chien, "A transmission line decoupling technique for enhancement of port isolation of dual-band MIMO antennas," *J. Electromagn. Waves Appl.*, vol.32, no.10, pp.1195–1211, 2018.
- [22] P.-L. Chi, C.-J. Lee, and T. Itoh, "A compact dual-band metamaterial-based rat-race coupler for a MIMO system application," *Proc. IEEE Int. Microw. Symp. Dig.*, Atlanta, GA, pp.667–670, June 2008.
- [23] D. Sibal, M.P. Abegaonkar, and S.K. Koul, "Highly isolated compact planar dual-band antenna with polarization/pattern diversity characteristics for MIMO terminals," *IEEE Antennas Wireless Propag. Lett.*, vol.18, pp.762–766, 2019.
- [24] H.V. Singh, D.V.S. Prasad, and S. Tripathi, "Dual-band MIMO antenna decoupling using vias based multipath decoupling circuit," *Microw. Opt. Technol. Lett.*, vol.64, no.4, pp.770–777, 2022.
- [25] X.-H. Li, "Decoupling of dual-band microstrip antenna array with hybrid resonant structure," *PIER Letters*, vol.94, pp.9–17, 2020.
- [26] J.-S. Hong and M.J. Lancaster, "Microstrip Filters for RF/Microwave Applications," New York, NY, USA: Wiley, 2001.
- [27] I.-H. Lin, M. DeVincentis, C. Caloz, and T. Itoh, "Arbitrary dual-band components using composite right/left-handed transmission lines," *IEEE Trans. Microw. Theory Tech.*, vol.52, no.4, pp.1142–1149, 2004.
- [28] F.-X. Liu and J.-C. Lee, "A dual-mode power divider with embedded meta-materials and additional grounded resistors," *Trans. Microw. Theory Tech.*, vol.69, no.8, pp.3607–3615, 2021.
- [29] Z. Wan, Q. Liu, W. Liu, D. Cheng, G. Du, and G. Li, "A compact dual-band frequency-dependent impedance transformer using two resizable shunt stubs," *Microw. Opt. Technol. Lett.*, vol.64, no.3, pp.440–445, 2021.
- [30] S.H. Chae, S.-k. Oh, and S.-O. Park, "Analysis of mutual coupling, correlations, and TARC in WiBro MIMO array antenna," *IEEE Antennas Wireless Propag. Lett.*, vol.19, pp.122–125, 2007.



**Xiang Xiong** received the M.S. degree in mechanical design and theory (major in electromagnetic compatibility) from Jimei University, Xiamen, China, in 2019. He is currently working toward the Ph.D. degree in Information and Communication Engineering at Harbin Engineering University, Harbin, China. His current research interests include MIMO antennas, metamaterial, and EMC design for the high-speed digital system.



**Wen Li** received the M.S. degree from Qingdao University of Technology, Shandong, China, in 2020. He is currently working toward the Ph.D. degree in Information and Communication Engineering at Harbin Engineering University, Harbin, China. His current research interests include circularly polarized antennas and MIMO antennas.



**Xiaohua Tan** received the B.S. degree in Mechanical Design Manufacture and Automation from Nanchang Hangkong University, Nanchang, China, in 2012, the M.S. degree in mechanical design and theory from Jimei University, Xiamen, China, in 2015, and the Ph.D. degree in Electronic Science and Technology from Beijing University of Posts and Telecommunications, Beijing, China, in 2021. His current research interests include circularly polarized antennas and MIMO antennas.



**Yusheng Hu** received the Ph.D. degree in mechanical and electronic engineering (major in EMC) from the Southeast University, Nanjing, China, in 2004. In Jan. 2004, He joined Jimei University, Xiamen, China, where he is currently a full professor and M.S. Candidate Advisor with the College of Marine Equipment and Mechanical Engineering. From Sep. 2004 to Sep. 2006, he was with Nanjing University of Aeronautics and Astronautics, Nanjing, China, as a post-doctoral research fellow. From Sep. 2010 to Mar. 2011, he was a Visiting Scholar with the EMC Laboratory, Missouri University of Science and Technology, Rolla, MO, USA. From Oct. 2014 to Sep. 2015, he studied at the Department of Electronics and Telecommunications, Politecnico Di Torino, Torino, Italy, as a visiting scholar. His research interests include SI, EMC/EMI analysis in high-speed digital systems and microwave antennas.